Med Biol Eng Comput (2012) 50:567–574
DOI 10.1007/s11517-012-0907-7

ORIGINAL ARTICLE

Quantitative color analysis for capillaroscopy image segmentation

Michela Goffredo · Maurizio Schmid · Silvia Conforto · Beatrice Amorosi · Tommaso D'Alessio · Claudio Palma

Received: 8 September 2011 / Accepted: 10 April 2012 / Published online: 25 April 2012

Abstract This communication introduces a novel approach for quantitatively evaluating the role of color space decomposition in digital nailfold capillaroscopy analysis. It is clinically recognized that any alterations of the capillary pattern, at the periungual skin region, are directly related to dermatologic and rheumatic diseases. The proposed algorithm for the segmentation of digital capillaroscopy images is optimized with respect to the choice of the color space and the contrast variation. Since the color space is a critical factor for segmenting low-contrast images, an exhaustive comparison between different color channels is conducted and a novel color channel combination is presented. Results from images of 15 healthy subjects are compared with annotated data, i.e. selected images approved by clinicians. By comparison, a set of figures of merit, which highlights the algorithm capability to correctly segment capillaries, their shape and their number, is extracted. Experimental tests depict that the optimized procedure for capillaries segmentation, based on a novel color channel combination, presents values of average accuracy higher than 0.8, and extracts capillaries whose shape and granularity are acceptable. The obtained results are particularly encouraging for future developments on the classification of capillary patterns with respect to dermatologic and rheumatic diseases.

M. Goffredo (✉) · M. Schmid · S. Conforto · T. D'Alessio
Department of Applied Electronics, University "Roma TRE", Rome, Italy
e-mail: goffredo@uniroma3.it

B. Amorosi
IFO San Gallicano Dermatology Institute, IRCCS, Rome, Italy

C. Palma
Department of Physics, University "Roma TRE", Rome, Italy

Keywords Capillaroscopy · Segmentation · Color analysis · Color space

1 Introduction

Nailfold capillaroscopy (NC) is a clinically recognized technique for non-invasive in vivo analysis of capillaries at the periungual skin region [3, 25]. The healthy capillary pattern typically appears as a uniform series of loops, hairpin-shaped, with homogeneous size and morphology. Alterations of the capillary structure are visible as enlargement and deformation of capillary loops, loss of capillaries, excessive capillary branching, and hemorrhages [7]. A large number of publications dealing with such anomalies demonstrated their relationship to pathologies such as systemic sclerosis [26], connective tissue diseases [21, 24] and dermatomyositis [9].

In literature, classifications of capillary morphological features were firstly presented with qualitative descriptions of whole NC pattern [14, 21, 32], and then with quantitative descriptions of individual capillaries [8, 19, 20, 38].

Although a large number of papers has been published on NC pattern description and classification, very few of them delved into software aids for the medical decision making issue. Since NC image interpretation is usually based on the clinician's visual observations, giving to the diagnosis an unknown degree of uncertainty, the design of ad hoc algorithms for NC image analysis is particularly appealing. The automatic image processing, in fact, allows collecting a number of descriptive parameters on a suitably large number of patients, thus contributing to the assessment of their relevance for each class of disease. Moreover, an automatic image annotation will simplify the process of image selection from medical care archives. For these

reasons, the present-day research goes in the direction of both extensive quantitative measurements and design of algorithms for the automatic pattern description and classification [2, 8, 10, 20, 21].

Digital NC images are usually noisy and characterized by very low contrast between the background and capillaries. For this reason, NC image processing is usually accomplished by transforming and analyzing the image onto a different color space where capillaries appear enhanced. However, literature presents some inconsistencies related to the color space transformation [5, 6, 15, 16, 22]. To this extent, a number of papers compared different color spaces [11, 23, 34], showing that they present different information enhancement and thus affect the segmentation output. However, in medical imaging context, there is not a complete work on the comparison of color spaces for segmenting NC images.

In order to overcome this limitation, this paper quantitatively evaluates the role of color space decomposition in NC segmentation. The proposed method for capillaries detection is optimized after an exhaustive comparison between different color channels, belonging to a large number of color spaces, and the optimum color channel combination is defined. A set of figures of merit, describing the segmentation quality is introduced by comparing the segmentation results with annotated data.

2 Methods

The overall approach for NC image analysis consists of four parts: capillary segmentation, clustering, description and classification. Output of the system is a suitable number of quantitative parameters, describing capillary distribution and morphology, which can be used for classification purposes.

This paper focuses on the segmentation phase (Fig. 1), aiming at optimizing it with respect to the color space decomposition.

2.1 Capillary segmentation

Let $RGB(x, y)$ be the three-channel color image gathered with a dermatoscope, and let $I(x, y)$ be the image obtained with the color space decomposition C. We represent with C both the one-channel projection of a chosen color space (e.g. R, G, or B of the RGB color space), and the linear combination of RGB color channels, i.e.:

$$\begin{aligned} I(x,y) &= C[RGB(x,y)] \\ &= \alpha \times R + \beta \times G + [1 - (\alpha + \beta)] \times B \end{aligned} \quad (1)$$

where the coefficients α and β are in $\mathbf{R}^1$.

Since capillary images contain a large amount of speckle noise, a 7×7 median filter is used to reduce it.

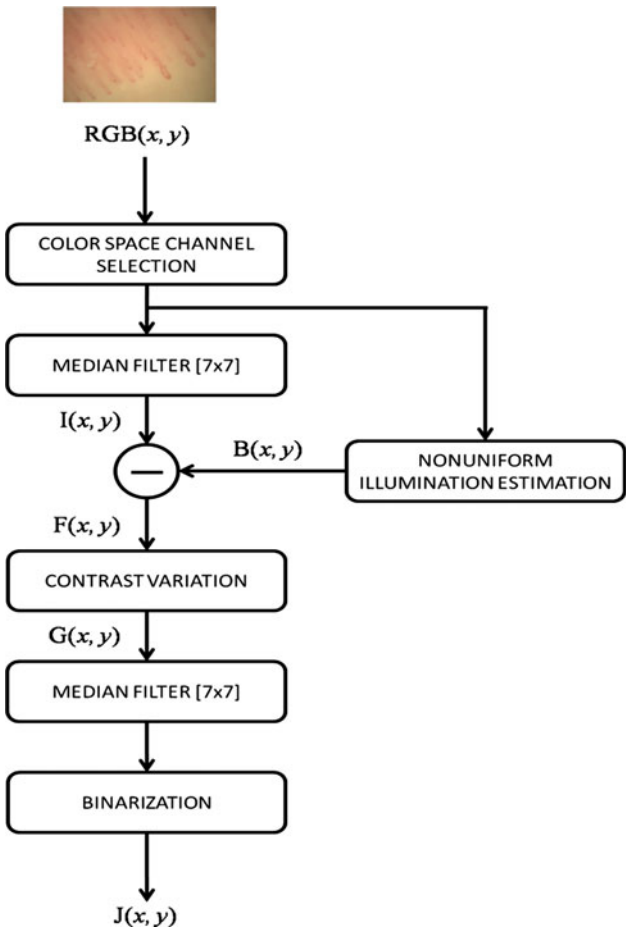

Fig. 1 Overview of the proposed segmentation method. NC image analysis is composed of four sections: capillary segmentation, clustering, description and classification. This paper aims at optimizing the segmentation phase with respect to the color space decomposition and the segmentation thresholds setting

Subsequently, a correction for non-uniform illumination is needed because the image presents a central lighter area due to the microscope light source (typically, with a Gaussian slowly decreasing distribution of intensity). The illumination correction is achieved by estimating $B(x, y)$, i.e. the image containing only the global differences of light, and subtracting it from $I(x, y)$:

$$F(x,y) = I(x,y) - B(x,y) \quad (2)$$

$B(x, y)$ is estimated by applying a morphological dilation operator to $I(x, y)$ using a disk with 25 pixels radius as structuring element.

After reducing noise and global light changes, $F(x, y)$ contrast has been changed with the classic gamma correction algorithm [12], where the point-wise operation is

$$G(x,y) = [F(x,y)]^{\gamma}. \quad (3)$$

Typically, the value of γ is empirically set by passing a calibration target with a full range of known luminance values

through the imaging system. However, such calibration is seldom available, or direct access to the imaging device is not possible and some a priori assumptions are thus needed [12]. In this paper, we established the optimal contrast correction, by evaluating the segmentation quality with respect to the value of γ.

The binary image $J(x, y)$, where 1-value pixels correspond to the segmented capillaries, is obtained by applying the Otsu binarization technique [27] to the smoothed version of $G(x, y)$, obtained by filtering it with a 7×7 median filter.

In the proposed algorithm, the choice of the color space decomposition C and the contrast variation γ is achieved through an optimization procedure which compares a set of figures of merit, described in the following, and calculated by comparing the segmentation results with annotated data.

2.2 Figures of merit

An objective and quantitative performance analysis of a segmentation algorithm can be achieved by means of a number of parameters, called figures of merit hereinafter, as described by [36]. In this contribution, we consider a set of 4 figures of merit, which highlight different properties of the segmented objects, similar to [4, 29, 35].

Firstly, the receiver operating characteristic (ROC curve) is determined [18]. If $\mathbf{X}(\gamma, C)$ is the set of pixels segmented as capillaries by the proposed method, with a chosen color space decomposition C and contrast variation γ, and $\mathbf{Y}$ is the set of pixels corresponding to capillaries in the annotated image, the classic statistical measures for sensitivity (SE) and specificity (SP) can be calculated as:

$$\begin{aligned} \mathrm{SE}(\gamma, C) &= \frac{a}{a+c} \\ \mathrm{SP}(\gamma, C) &= \frac{d}{b+d} \end{aligned} \tag{4}$$

where a is the number of pixels in $\mathbf{X} \cap \mathbf{Y}$, b is the number of pixels in $\mathbf{X}$ not belonging to $\mathbf{Y}$, c is the number of pixels of $\mathbf{Y}$ not belonging to $\mathbf{X}$ and d is the number of pixels outside $\mathbf{X}$ and $\mathbf{Y}$. From the ROC curve, the area under the curve (AUC) can be extracted as an indicator of the algorithm accuracy, which depends on the color space decomposition C only [13], i.e. independently from the contrast variation γ. The figure of merit which has been considered for describing the algorithm performance in terms of sensitivity and specificity by varying both C and γ is the average accuracy (AA):

$$\mathrm{AA}(\gamma, C) = \frac{\mathrm{SE}(\gamma, C) + \mathrm{SP}(\gamma, C)}{2}. \tag{5}$$

The second figure of merit is the spatial overlap measure defined by [33] and successively applied in [1, 4] for a comparison between segmented images. The Tanimoto index (TN) is defined by:

$$\begin{aligned} \mathrm{TN}(\gamma, C) &= \frac{|\mathbf{X}(\gamma, C) \cap \mathbf{Y}| + \left|\overline{\mathbf{X}(\gamma, C) \cup \mathbf{Y}}\right|}{|\mathbf{X}(\gamma, C) \cup \mathbf{Y}| + \left|\overline{\mathbf{X}(\gamma, C) \cap \mathbf{Y}}\right|} \\ &= \frac{a+d}{a+2b+2c+d} \end{aligned} \tag{6}$$

which is equal to one if region $\mathbf{X}(\gamma, C)$ and $\mathbf{Y}$ overlap and zero if they are disjoint and occupy the entire image.

The analysis of AA and TN indexes is a good procedure to quantify the performance of an image segmentation algorithm. However, these figures compare only the number of pixels and no information about the position of misclassified/correctly classified pixels is included. Since NC image analysis aims at extracting a set of pattern descriptors, it appears relevant to compare figures of merit that include this information, introducing the shape of the extracted loops into the quality metrics.

To this extent, we introduce Pratt's figure of merit (FOM), which has been widely used in image processing [17, 30], since it measures the deviation of the obtained capillary edges from the annotated edges:

$$\mathrm{FOM}(\gamma, C) = \frac{1}{\max(E_X(\gamma, C), E_Y)} \sum_{i=1}^{E_X(\gamma, C)} \frac{1}{1 + \rho \cdot d^2(i)} \tag{7}$$

where $E_X(\gamma, C)$ is the set of edge points detected by the proposed algorithm, E_Y is the set of edge points in the annotated image, ρ is a scaling factor (usually set to 0.01), and $d(i)$ is the Euclidean distance of the detected edge pixel from the nearest ideal edge position.

The fourth figure of merit includes information on the number of extracted capillaries into the image. It is the Cardenes's connectivity coefficient (CCc), defined by [4] with

$$\mathrm{CCc}(\gamma, C) = 2 \cdot \frac{\min\{N_X(\gamma, C), N_Y\}}{N_X(\gamma, C) + N_Y} \tag{8}$$

where $N_X(\gamma, C)$ is the number of capillaries that have been segmented with the proposed approach and N_Y is the actual number of capillaries. Therefore, CCc includes information about the connectivity of the segmented objects since it is associated to the amount of granularity of the image.

Therefore, given a set of γ values and a number of color decomposition C, the optimum values γ^{opt} and C^{opt} are chosen as the couple of values corresponding to the maximum amplitude value of the 4D vector $\vartheta(\gamma, C) = [\mathrm{AA}, \mathrm{TN}, \mathrm{FOM}, \mathrm{CCc}\,]$. If C is the color combination procedure, the optimization method includes also the choice of α and β coefficients of Eq. (1).

2.3 Evaluation procedure

Experiments have been conducted on 15 NC images from 15 healthy subjects recruited, after consent, by IFO San Gallicano Dermatology Institute (IRCCS), Rome, Italy.

Images have been gathered with a Dermascope of Medici Medical s.r.l., composed of a 300× microscope, a video camera and the acquisition software. Calibration via USAF test target returned a 1.3 × 1.0 mm FOV with a minimum resolved distance on the image of 3.9 μm. As the image consists of 753 × 560 pixels, each pixel has dimensions 1.8 μm, and the minimum resolved spot is of 2 × 2 pixels.

Annotated data has been produced for each image, consisting of hand segmentation done by a set of expert human operators outlining the boundary of each apparent capillary in each image. Clinicians gave their approval to the annotated dataset.

The original color images have been decomposed into the following color spaces: RGB, Lab, YCbCr, YUV, HSV and the color channel combination previously described.

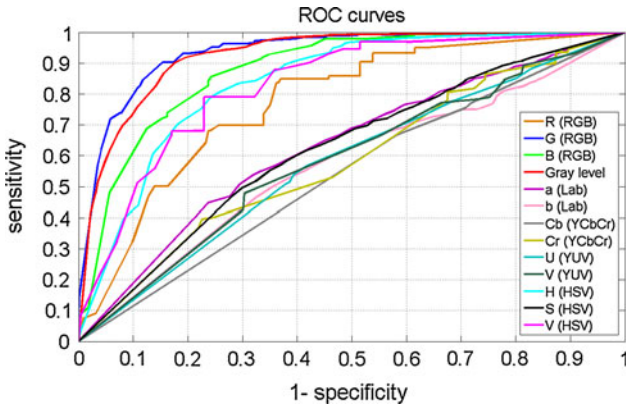

Fig. 2 ROC curves of each color space channel, obtained by calculating sensitivity and specificity mean values by varying the γ value between 0.05 and 2. Among the traditional color space components, the *green* channel of RGB color space and the *grey*-level image present the best performance (color figure online)

Each image has been processed separately by varying the γ value between 0.05 and 2 with steps of 0.05. The α and β coefficients have been varied from −3 to 1 and from −1 to 5, respectively (steps of 0.1). Sensitivity, specificity, and the figures of merit previously introduced have been extracted by comparing the obtained segmentation with the annotated data.

3 Results

Sensitivity and specificity mean values are shown in the ROC curves depicted in Fig. 2, for all the single color channels, where grey level is the luminance channel. The application of the proposed NC segmentation method on the green channel shows the best performance, as predictable.

The analysis of color channel combination is reported in Fig. 3, where the left panel depicts the mean AUC values with respect to α and β coefficients.

AUC values with regard to the single color channels confirm the results shown in the ROC curves of Fig. 2. The green channel presents an AUC value of 0.93 and sensitivity and specificity values, corresponding to the maximum value of AA in Fig. 5a, of 0.84 and 0.90, respectively. The grey-level image also has good accuracy (sensitivity and specificity of 0.82 and 0.90 when AA is maximum), while the blue channel of RGB color space is acceptable (sensitivity and specificity of 0.75 and 0.85 when AA is maximum). Results obtained with the other color channels are not of interest since AUCs are lower than 0.8. In this panel, AUC obtained with the optimized color combination, called C_{combo}, is also reported, and its

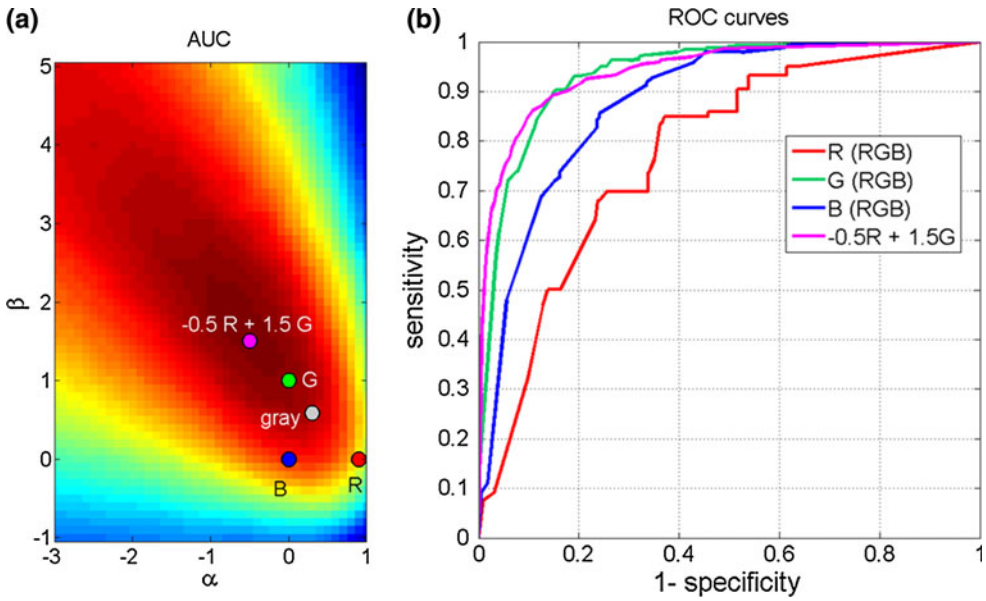

Fig. 3 Quantitative evaluation of the linear combination of the RGB color channels. **a** AUC values with respect to α and β coefficients. Both the *green* channel and the *grey*-level image present good accuracy, but AUC obtained with the optimized color combination C_{combo}, is higher (0.94). **b** Compares the C_{combo} ROC curve with the ones obtained with the single RGB channels: difference between the *green* channel, weighted by 1.5, and the *red* channel, weighted by −0.5, increases the performance of the proposed segmentation algorithm (color figure online)

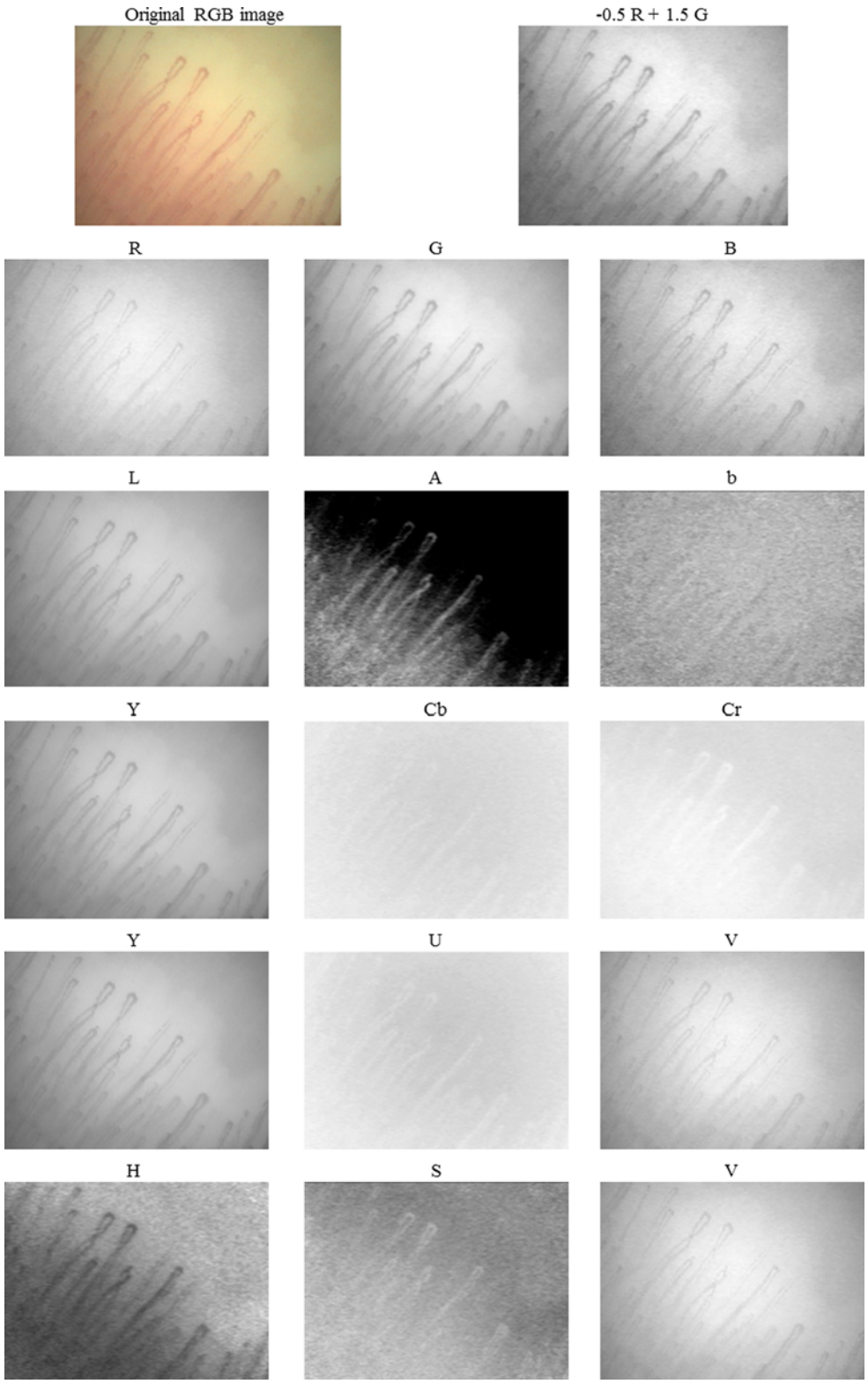

Fig. 4 Example of NC image (subject 6) represented in each channel of the color spaces and with the proposed color combination C_{combo}, obtained with $\alpha = -0.5$ and $\beta = 1.5$

maximum value (0.94) is obtained with $\alpha = -0.5$ and $\beta = 1.5$. This value is higher than the one obtained with the green channel.

The right panel, which compares the C_{combo} ROC curve with the ones obtained with the single RGB channels, reports that the difference between the green channel,

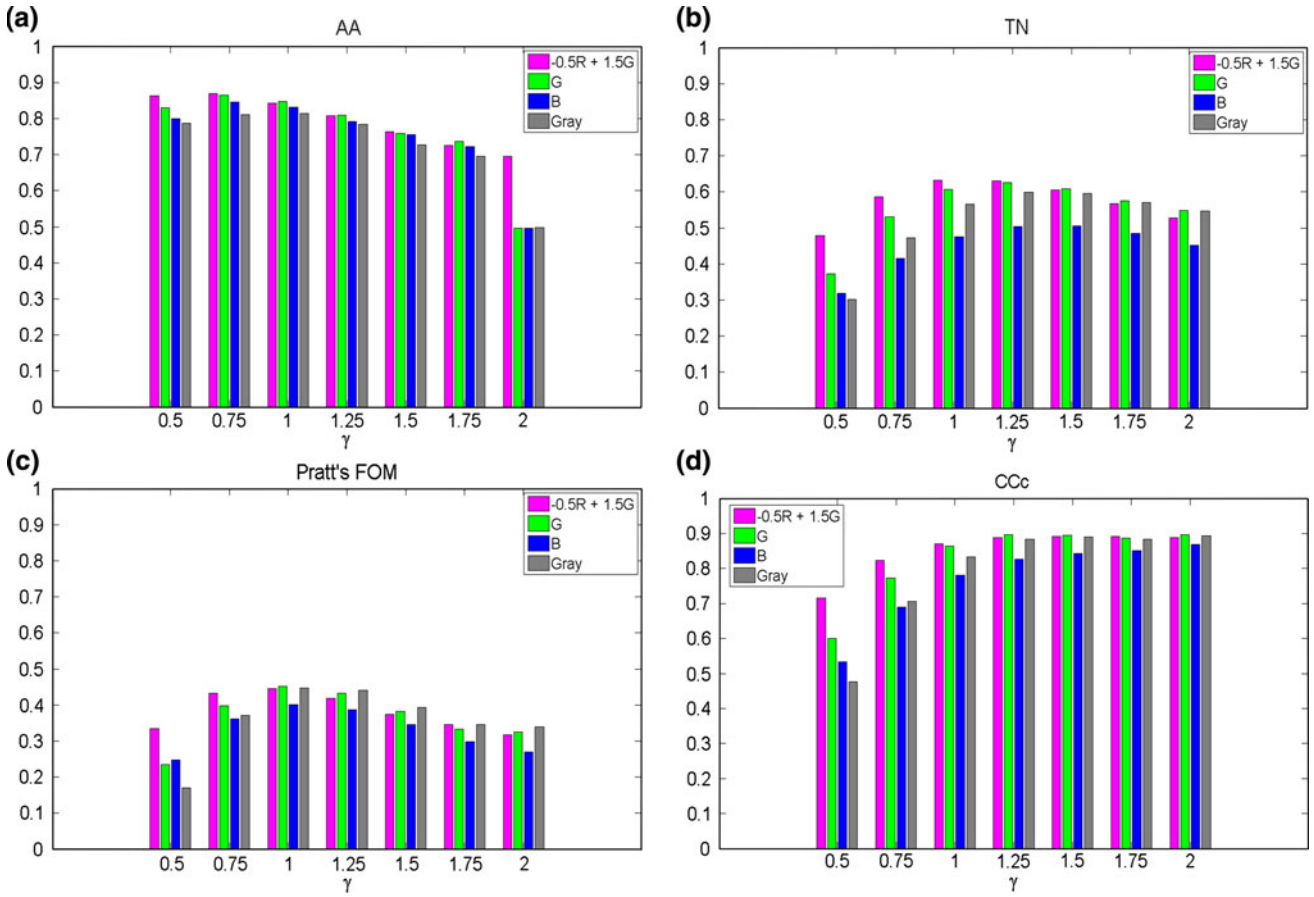

Fig. 5 Figures of merit which highlight different properties of the segmented objects with respect to color component and γ value: the average accuracy AA depicts algorithm performance in terms of sensitivity and specificity (**a**); the Tanimoto figure of merit TN is a spatial overlap measure (**b**); Pratt's figure of merit FOM measures the deviation of the obtained capillary edges from the annotated edges (**c**); CCc figure of merit includes information about granularity of the segmented image (**d**)

weighted by 1.5, and the red channel, weighted by -0.5, increases the performance of the proposed segmentation algorithm. Values of sensitivity and specificity with C_{combo} are 0.87 and 0.89, respectively.

Figure 4 shows an example of NC image in each channel of the considered color spaces and the image obtained with the combination C_{combo}.

Figures of merit, describing the capability of the proposed segmentation algorithm in terms of overlapped area, edge distance and image granularity, have been also extracted for the three color channels whose AUC is higher (i.e. G, B, grey), and for C_{combo}. Figure 5 shows the mean values of AA, TN, FOM and CCc with respect to γ values.

Figures of merit confirm that C_{combo} presents the best performance, with AA of 0.87 and TN index of 0.63. The maximum values of FOM and CCc are 0.45 and 0.89, respectively, showing better behavior than single color channels in extracting capillary's edge and granularity.

Regarding the optimization procedure of the contrast variation algorithm, it emerges that the application of the gamma correction algorithm with a value of 1.25 corresponds to the highest values of TN, FOM and CCc. The result of the optimization method, which is based on the maximization of the 4D vector $\vartheta(\gamma, C) = [\text{AA, TN, FOM, CCc}]$, is $\gamma = 1.25$.

4 Discussion

Because of the noisy and low-contrast nature of digital NC images, their processing is usually accomplished by transforming and analyzing the image onto a different color space where capillaries appear enhanced [37].

Although the scientific community found the necessity to explore NC digital image processing for the automatic pattern classification, literature presents some inconsistencies related to the color space transformation: Kwasnicka and Paradowski [22] were the first to introduce a method for the automatic segmentation and description of NC images where both the RGB and HSV color spaces have been analyzed; Chia-Hsien et al. [5, 6] introduced a classification framework based on grey-level images; and

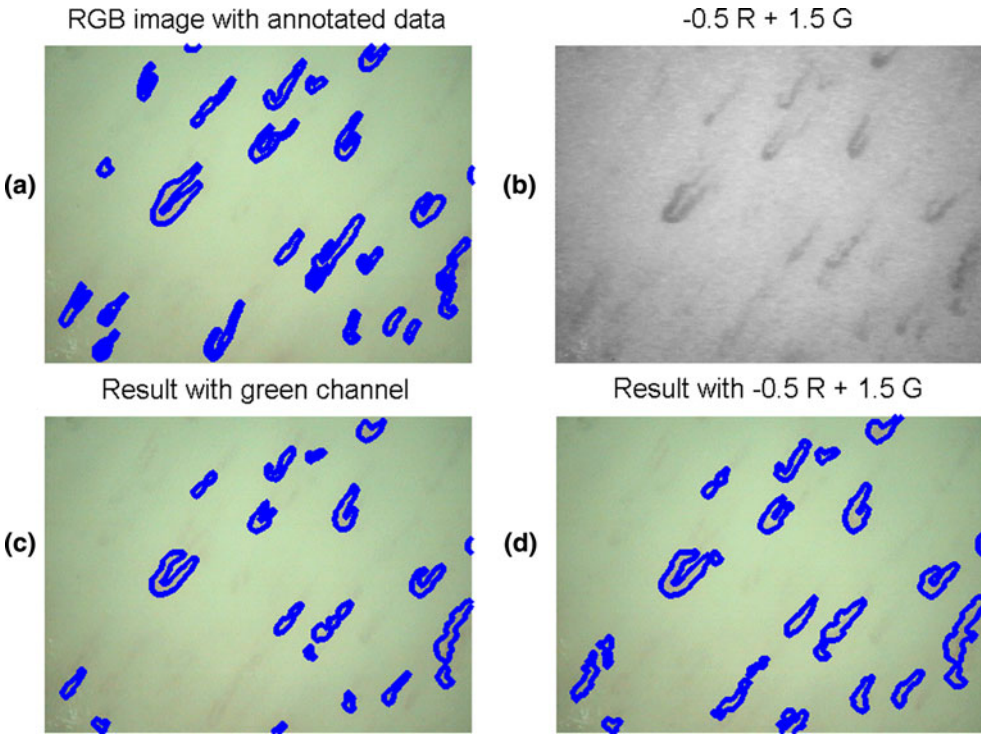

Fig. 6 Example of RGB image with annotated data (**a**), the proposed color combination image, with $\gamma = 1.25$ (**b**) and the segmentation results obtained by applying the proposed method on the green channel (**c**) and on the proposed C_{combo} (**d**)

Riao-Rojas et al. [31] presented a method for illumination correction, image enhancing and segmentation, based on the analysis of YCbCr, Lab and HSV color spaces.

Since the choice of the color space transformation is not completely agreed, this paper quantitatively evaluates the role of color space decomposition in NC segmentation by means of a set of figures of merit.

From the analysis of the ROC curves of Fig. 2, it emerges that, among the traditional color space components, the green channel of RGB color space presents the best performance, as empirically chosen by many authors [22, 28].

By merging different color channels, we found that a not negligible increase in performance can be obtained with a specific linear combination of them.

This optimized combination yields the best values not only with respect to the AUC values, but also by taking into account all the figures of merit. This can be also verified by looking at Fig. 6, which compares the segmentation quality, obtained with the green channel, against the one obtained with C_{combo} on a sample NC image.

As it can be seen, the green channel presents a slightly smaller amount of information since the segmented capillaries overlap the annotated data only partially; the position of false positive pixels is not close to true positive locations and the number of extracted capillaries is not the same as the actual one.

Regarding the optimization procedure of the contrast variation algorithm, it emerges that the application of the gamma correction algorithm with a value of 1.25 corresponds to the highest values of TN, FOM and CCc. On the other hand, AA shows higher value with a γ value of 0.75. This can be justified by the fact that AA includes only the number of segmented pixels with respect to the annotated data and no information about shape and granularity of the extracted capillaries is contained.

Results highlight the algorithm capability to correctly segment capillaries, their shape and their number. Data show that, with the segmentation algorithm here implemented, the optimized combination of the RGB color channels reported in this study presents the highest segmentation quality.

In conclusion, results confirm that color space is a critical factor for segmenting low-contrast NC images. For this reason, this manuscript describes an exhaustive comparison between different color channels and presents a novel approach for NC image segmentation, optimized with respect to the choice of the color space and the contrast variations.

Acknowledgments We gratefully acknowledge the support of IFO San Gallicano Dermatology Institute, IRCCS, Rome, Italy. In particular, we thank A. Di Carlo and M. Ardigò for the time patiently spent with us.

References

1. Alonso F, Algorri M, FIores-Mangas F (2004) Composite index for the quantitative evaluation of image segmentation results. In: Engineering in Medicine and Biology Society, 2004. IEMBS '04.

26th Annual International Conference of the IEEE, San Francisco, pp 1794–1797
2. Bezemer R, Dobbe JG, Bartels SA, Christiaan Boerma E, Elbers PW, Heger M, Ince C (2011) Rapid automatic assessment of microvascular density in sidestream dark field images. Med Biol Eng Comput 49(11):1269–1278
3. Bollinger A, Flagrell B (1990) Clinical capillaroscopy—a guide to its use in clinical research and practice. Hogrefe Huber, Toronto and Lewiston
4. Cardenes R, De Luis-Garcia R, Bach-Cuadram M (2009) A multidimensional segmentation evaluation for medical image data. Comput Methods Programs Biomed 96(2):108–124
5. Chia-Hsien W, Tsu-Yi H, Wei-Duen L, Joung-Liang L, Der-Yuan C, Kuan-Ching L (2008) A novel method for classification of high-resolution nailfold capillary microscopy images. In: First IEEE International Conference on Ubi-Media Computing, pp 513–518
6. Chia-Hsien W, Wei-Duen L, Kuan-Ching L (2007) Classification framework for nailfold capillary microscopy images. In: IEEE Region 10 Conference TENCON 2007, pp 1–4
7. Cutolo M, Pizzorni C, Secchi M, Sulli A (2008) Capillaroscopy. Best Pract Res Clin Rheumatol 22(6):1093–1108
8. Cutolo M, Sulli A, Pizzorni C, Accardo S (2000) Nailfold videocapillaroscopy assessment of microvascular damage in systemic sclerosis. J Rheumatol 27:155–160
9. De Visser M, Emslie-Smith A, Engel A (1989) Early ultrastructural alterations in adult dermatomyositis: capillary abnormalities precede other structural changes in muscle. J Neurol Sci 94:1
10. Dobbe JG, Streekstra GJ, Atasever B, van Zijderveld R, Ince C (2008) Measurement of functional microcirculatory geometry and velocity distributions using automated image analysis. Med Biol Eng Comput 46(7):659–670
11. Fang G, Kwok N (2009) Image segmentation using adaptively selected color space. In: 2009 IEEE International Conference on Robotics and Biomimetics (ROBIO), pp 1838–1843
12. Farid H (2001) Blind inverse gamma correction. IEEE Trans Image Process 10(10):1428–1433
13. Fawcett T (2006) An introduction to ROC analysis. Pattern Recognit Lett 27(8):861–874
14. Gibson WC, Bosley HJSGR (1956) Photomicrographic studies of the nailbed capillary networks in human control subjects. J Nerv Ment Dis 219:219–231
15. Goffredo M, Schmid M, Conforto S, Carli M, Neri A, D'Alessio T (2009) Markerless human motion analysis in Gauss-Laguerre transform domain: an application to sit-to-stand in young and elderly people. IEEE Trans Inf Technol Biomed 13(2):207–216
16. Goffredo M, Schmid M, Conforto S, D'Alessio T (2005) A markerless sub-pixel motion estimation technique to reconstruct kinematics and estimate the centre of mass in posturography. Med Eng Phys 28(7):719–726
17. Gudmundsson M, El-Kwae E, Kabuka M (1998) Edge detection in medical images using a genetic algorithm. IEEE Trans Med Imaging 17(3):469–474
18. Hanley JA, McNeil BJ (1982) The meaning and use of the area under a receiver operating characteristic (ROC) curve. Radiology 143(1):29–36
19. Hu Q, Mahler F (1999) New system for image analysis in nailfold capillaroscopy. Microcirculation 6:227–235
20. Jones B, Oral M, Morris C, Ring EFJ (2001) A proposed taxonomy for nailfold capillaries based on their morphology. IEEE Trans Med Imaging 20(4):333–341
21. Kabasakal Y, Elvins D, Ring E, McHugh N (1996) Quantitative nailfold capillaroscopy findings in a population with connective tissue disease and in normal healthy controls. Ann Rheum Dis 55:507–512
22. Kwasnicka H, Paradowski M (2007) Capillaroscopy image analysis as an automatic image annotation problem. In: 6th International Conference on Computer Information Systems and Industrial Management Applications, pp 266–27
23. Kwok N, Ha Q, Fang G (2009) Effect of color space on color image segmentation. CISP '09. In: 2nd International Congress on Image and Signal Processing, pp 1–5
24. Lee P, Leung F, Alderdice C, Armstrong S (1983) Nailfold capillary microscopy in the connective tissue diseases: a semiquantitative assessment. J Rheumatol 10(6):930–938
25. Maricq HR, Maize JC (1982) Nailfold capillary abnormalities. Clin Rheum Dis 8(2):455–478
26. Maricq M (1988) Raynauds phenomenon and microvascular abnormalities in scleroderma (systemic sclerosis). In: Black MJ (ed) Systemic sclerosis: scleroderma, pp 151–66
27. Otsu N (1979) A threshold selection method from gray-level histograms. IEEE Trans Syst Man Cybern 9(1):62–66
28. Paradowski M, Kwasnicka H, Borysewicz K (2009) Avascular area detection in nailfold capillary images. In: International Multiconference on Computer Science and Information Technology, IMCSIT '09, pp 419–424
29. Pichon E, Tannenbaum A, Kikinis R (2004) A statistically based flow for image segmentation. Med Image Anal 8(3):267–274
30. Pratt WK (1978) Digital image processing. Wiley, New York
31. Riao-Rojas J, Prieto-Ortiz F, Morantes L, Sanchez-Camperos E, Jaramillo-Ayerbe F (2007) Segmentation and extraction of morphologic features from capillary images. Sixth Mexican International Conference on Artificial Intelligence—Special Session, MICAI 2007, pp 148–159
32. Rouen LR, Terry EN, Doft BH, Redisch W (1972) Classification and measurement of surface microvessels in man. Microvasc Res 4:285–292
33. Tanimoto T (1958) An elementary mathematical theory of classification and prediction. IBM internal rep, New York
34. Wang Yuedong XH (2009) Studies on color space selection and methods of segmentation quality evaluation. In: 1st International Conference on Information Science and Engineering (ICISE), pp 1437–1440
35. Wesolkowski S, Jernigan M, Dony R (2000) Comparison of color image edge detectors in multiple color spaces. In: International Conference on Image Processing, vol 2, pp 796–799
36. Zhang Y (1996) A survey on evaluation methods for image segmentation. Pattern Recognit 29(8):1335–1346
37. Zhanwu X, Miaoliang Z (2006) Color-based skin detection: survey and evaluation. In: Proceedings of the 12th International Conference on Multi-Media Modelling, vol 10, Beijing
38. Zhong J, Asker CL, Salerud EG (2000) Imaging, image processing and pattern analysis of skin capillary ensembles. Skin Res Technol 6:45–57